To appear in Journal of Applied Mechanics (DOI: 10.1115/1.4066285)

Interplay between Nucleation and Kinetics in Dynamic Twinning

Janel Chua,[1,*] Vaibhav Agrawal,[2] Noel Walkington,[3] George Gazonas,[4] and Kaushik Dayal[5,3,6]

[1]*Los Alamos National Laboratory*
[2]*Apple Inc.*
[3]*Center for Nonlinear Analysis, Department of Mathematical Sciences, Carnegie Mellon University*
[4]*DEVCOM Army Research Laboratory, Attn: FCDD-RLW-MB, Aberdeen Proving Ground, MD 21005, USA*
[5]*Department of Civil and Environmental Engineering, Carnegie Mellon University*
[6]*Department of Mechanical Engineering, Carnegie Mellon University*

(Dated: August 20, 2024)

In this work, we apply a phase-field modeling framework to elucidate the interplay between nucleation and kinetics in the dynamic evolution of twinning interfaces. The key feature of this phase-field approach is the ability to transparently and explicitly specify nucleation and kinetic behavior in the model, in contrast to other regularized interface models. We use this to study 2 distinct problems where it is essential to explicitly specify the kinetic and nucleation behavior governing twin evolution.

First, we study twinning interfaces in 2-d. When these interfaces are driven to move, we find that significant levels of twin nucleation occur ahead of the moving interface. Essentially, the finite interface velocity and the relaxation time of the stresses ahead of the interface allows for nucleation to occur before the interface is able to propagate to that point. Second, we study the growth of needle twins in antiplane elasticity. We show that both nucleation and anisotropic kinetics are essential to obtain predictions of needle twins. While standard regularized interface approaches do not permit the transparent specification of anisotropic kinetics, this is readily possible with the phase-field approach that we have used here.

1. Introduction

Twinning and structural phase transformations are important phenomena in materials science and solid-state physics due to the significant role they play in influencing the properties and behavior of materials [38]. Some specific areas of applications are in shape memory alloys (SMAs) where the reversible twinning and detwinning of SMAs are responsible for their unique shape-changing behavior [4]. In other instances, structural phase transformations allow for tailoring material properties to specific applications, for instance in nanotwinned metals [28, 29, 33, 43].

The microstructure of the materials in which twinning or phase transformations occur typically consists of homogeneously deformed regions separated by interfaces across which the deformation varies extremely rapidly. Many interesting material phenomena under extreme conditions are governed by the nucleation, motion and response of the interfaces [4, 21]. It is therefore important to be able to accurately model propagating interfaces in a dynamic setting, particularly when inertia plays a significant role since these interfaces move at velocities comparable to the sonic speeds.

Related prior work. Continuum models for dynamic twin interface nucleation and propagation fall into two broad classes: sharp interface models [1, 3, 27, 40, 44, 45] and regularized interface models [2, 17, 24, 39, 48, 49]. In the case of the former, numerical computations are extremely challenging as sharp interfaces require expensive tracking algorithm in a numerical discretization. This is essentially infeasible when one expects numerous evolving and interacting interfaces, and thus the sharp interface approaches are not widely applied.

Regularized interfaces on the other hand do not require explicit tracking of the interfaces, which makes the numerical methods much simpler and enables application to complex settings. Phase-field models, wherein an additional regularized phase field variable is introduced to account for material transformations, have been widely applied to problems such as structural phase transformations, fracture, poromechanics, and dislocation dynamics, e.g. [7, 12, 14, 16, 18, 20, 26, 30–32, 37]. However, these methods also have significant shortcomings. Particularly, the dependence of the kinetics and nucleation of interfaces on the structure of the material model is completely opaque. Further, the range of material responses that can be obtained is highly constrained. Furthermore, the nucleation and the kinetics of interfaces are physically distinct processes from the atomic perspective, but standard phase-field models are unable to transparently distinguish these processes. One consequence of these shortcomings is that even in the simplest 1-d case, the precise critical condition at which nucleation occurs is completely opaque. Consequently, it is essentially impossible in practice to formulate a model to obtain a desired nucleation response. All of this is in sharp contrast to sharp interface models wherein the nucleation and kinetics of interfaces can be transparently specified in the model.

To retain the computational ease of phase-field models and at the same time obtaining the transparent physical structure of sharp-interface models, we recently proposed a phase-field modeling approach that enables the transparent specification of

* janelchua@lanl.gov

interface nucleation and kinetics as input to the model [5, 6, 11]. The key elements of this approach are, first, formulating an energy density that separates nucleation from kinetics; and, second, formulating a geometrically-motivated interface conservation principle to govern the nucleation and kinetics of interface. In this conservation principle, the kinetics of interfaces is governed by a transport term and the nucleation of interfaces is governed by a source term, and each of these contribution can be transparently and independently specified.

Contributions of this paper. In this paper, we use the phase-field approach described above to study the interplay between kinetics and nucleation in dynamic twinning. Specifically, we study 2 distinct problems where it is essential to be able to explicitly specify the kinetic and nucleation behavior governing twin evolution.

First, we study twinning interfaces in 2-d. When these interfaces are driven to move, we find that significant levels of twin nucleation occur ahead of the moving interface. Essentially, the finite interface velocity and the relaxation time of the stresses ahead of the interface allows for nucleation to occur before the interface is able to propagate to that point. Second, we study the growth of needle twins in antiplane elasticity. We show that both nucleation and anisotropic kinetics are essential to obtain predictions of needle twins. While standard regularized interface approaches do not permit the transparent specification of anisotropic kinetics, this is readily possible with the phase-field approach that we have used here.

2. Model Formulation

2.A. Notation

We use $\boldsymbol{x}_0$ and $\boldsymbol{x}(\boldsymbol{x}_0)$ to denote the reference and deformed configurations, and the displacement is denoted $\boldsymbol{u}(\boldsymbol{x}_0) := \boldsymbol{x}(\boldsymbol{x}_0) - \boldsymbol{x}$. We work completely in the Lagrangian setting for simplicity, while noting that there can be several advantages to an Eulerian approach in the large deformation setting [13, 23, 35, 36]. We use ∇ and div to denote the gradient and divergence with respect to $\boldsymbol{x}_0$, and superposed dots to denote time derivatives. The deformation gradient is denoted by $\boldsymbol{F} := \nabla \boldsymbol{x}$, the strain by $\boldsymbol{E} := \frac{1}{2}\left(\boldsymbol{F}^T\boldsymbol{F} - \boldsymbol{I}\right)$, the spatial velocity gradient by $\boldsymbol{L} = \dot{\boldsymbol{F}}\boldsymbol{F}^{-1}$, and the first Piola-Kirchoff stress by $\boldsymbol{P}$. We define $\boldsymbol{D} := \frac{1}{2}\left(\boldsymbol{L} + \boldsymbol{L}^T\right)$, $J := \det \boldsymbol{F}$, and use ϕ to denote the phase field.

We define a regularized indicator function $H_l(\cdot)$ that smoothly transitions — over an interval of order l — from 0 to 1 when the argument changes from negative to positive. For specificity, we use the form $H_l(x) = \frac{1}{2}\left(1 + \tanh\left(\frac{x}{l}\right)\right)$ and $l = 0.1$.

The domain and its boundary are denoted by Ω and $\partial\Omega$ respectively.

2.B. Governing Equations

We use the standard free energy of the form:

$$E[\boldsymbol{u}, \phi] = \int_\Omega \left(W(\boldsymbol{F}, \phi) + \frac{\alpha}{2}|\nabla\phi|^2\right) \, \mathrm{d}\Omega \tag{2.1}$$

where W is the elastic energy density and α is the phase-field regularization parameter. We use $\alpha = 1.2 \times 10^{-4}\mathrm{m}$.

We follow [5, 6] in setting W to have the general form:

$$W(\boldsymbol{F}, \phi) = H_l(0.5 - \phi)\, W_1(\boldsymbol{F}) + H_l(\phi - 0.5)\, W_2(\boldsymbol{F}) \tag{2.2}$$

where W_1 and W_2 correspond to the elastic energy density in phase 1 ($\phi < 0.5$) and phase 2 ($\phi > 0.5$) respectively. As described in [5, 6], this form contributes to a transparent separation between kinetics and nucleation. For specificity, we choose $W_i(\boldsymbol{F}) = \frac{1}{2}(\boldsymbol{E} - \boldsymbol{E}_i) : \boldsymbol{C}_i : (\boldsymbol{E} - \boldsymbol{E}_i), i \in \{1, 2\}$, where $\boldsymbol{C}_i$ is the 4-th order elastic modulus tensor.

The evolution equations associated with this energy are [5, 6]:

$$\text{Momentum balance: } \rho\ddot{\boldsymbol{u}} = \operatorname{div} \boldsymbol{P} \tag{2.3a}$$

$$\text{Phase evolution: } \dot{\phi} = |\nabla\phi|\hat{v}(f) + G(\boldsymbol{E}, \phi) \tag{2.3b}$$

The evolution equation for ϕ was proposed in [8], and was shown to correspond to a balance law for interfaces [6, 25]. G originates as a source term in that balance law, and in this work is used to induce the nucleation of an appropriate phase when the system evolves to access nonphysical regions of the energy landscape [11]. The specific forms of G will be described in later sections.

The phase velocity $\hat{v}(f)$ is a function of the driving force f, which is the negative of the functional derivative of E with respect to ϕ:

$$f := -\frac{\partial W}{\partial \phi} + \alpha \operatorname{div} \nabla\phi \tag{2.4}$$

[5, 6, 11] provide conditions that G and $\hat{v}(f)$ must satisfy for consistency with the 2-nd law of thermodynamics [30, 37].

The Piola-Kirchoff stress is composed of an elastic part and a viscous dissipative part: $\boldsymbol{P} = \boldsymbol{P}_{elas} + \boldsymbol{P}_{vis}$. The elastic part is given by $\boldsymbol{P}_{elas} = \left(\dfrac{\partial W(\boldsymbol{F}, \phi)}{\partial \boldsymbol{F}}\right)$. The viscous stress is assumed to follow a frame-invariant Newtonian model with a linear relation between the Cauchy stress and $\boldsymbol{D}$ [42]:

$$\boldsymbol{\sigma}_{vis} = \eta \boldsymbol{D} = \frac{\eta}{2}\left(\boldsymbol{L} + \boldsymbol{L}^T\right) \implies \boldsymbol{P}_{vis} = J\boldsymbol{\sigma}_{vis}\boldsymbol{F}^{-T} = \frac{\eta}{2} J\left(\dot{\boldsymbol{F}}\boldsymbol{F}^{-1} + \boldsymbol{F}^{-T}\dot{\boldsymbol{F}}^T\right)\boldsymbol{F}^{-T} \tag{2.5}$$

where η is the viscosity.

2.C. Finite Element Implementation

Weuse the finite element method (FEM) to solve numerically using the using the open-source FEM package FEniCS [9, 34]. We use a mixed finite element formulation and discretize (2.3a), (2.4), and (2.3b). The mixed formulation is required because the higher derivatives in f from (2.4) cannot be treated in the usual way using integration-by-parts, because f appears inside the response function $\hat{v}(f)$. The weak form is then:

$$\int_\Omega \rho\ddot{\boldsymbol{u}} \cdot \tilde{\boldsymbol{u}} \,\mathrm{d}\Omega = -\int_\Omega \boldsymbol{P} : \nabla\tilde{\boldsymbol{u}} \,\mathrm{d}\Omega + \int_{\partial\Omega} (\boldsymbol{P}\hat{\boldsymbol{n}}) \cdot \tilde{\boldsymbol{u}} \,\mathrm{d}S \tag{2.6a}$$

$$\int_\Omega f\tilde{f} \,\mathrm{d}\Omega = \int_\Omega \left(-\left(\frac{\partial W}{\partial \phi}\right)\tilde{f} - \alpha\nabla\phi\cdot\nabla\tilde{f}\right) \mathrm{d}\Omega + \int_{\partial\Omega} \alpha\tilde{f}\nabla\phi\cdot\hat{\boldsymbol{n}} \,\mathrm{d}S \tag{2.6b}$$

$$\int_\Omega \dot{\phi}\tilde{\phi} \,\mathrm{d}\Omega = \int_\Omega \left(|\nabla\phi|\hat{v}(f) + G(\boldsymbol{E}, \phi)\right)\tilde{\phi} \,\mathrm{d}\Omega \tag{2.6c}$$

where $\boldsymbol{u}$ and the corresponding test function $\tilde{\boldsymbol{u}}$ belong to the space of vector-valued functions that are piecewise linear; and f and ϕ, with the corresponding test functions $\tilde{f}$ and $\tilde{\phi}$, belong to the space of scalar-valued functions that are piecewise linear.

The boundary conditions for momentum balance (2.6a) are the standard displacement or traction prescribed, and the boundary condition for phase evolution (2.6c) is the standard variational condition $\nabla\phi\cdot\hat{\boldsymbol{n}} = 0$ [49] on the entire boundary.

The momentum balance and the phase evolution are evolved in time using the implicit Newmark method and the implicit Euler method respectively.

3. Nucleation Ahead of the Twin Interface at High Rates

We apply the model described in Section 2 to predict the motion of a flat twin interface in a 2-d nonlinear elastic setting, and specifically study the role of phase nucleation when inertial effects are significant.

3.A. Elasticity and Geometry of Twinning

Following [6], we consider twinning defined by the following transformation stretch tensors:

$$\boldsymbol{U}_1 = \begin{bmatrix} a & 0 \\ 0 & b \end{bmatrix}, \quad \boldsymbol{U}_2 = \begin{bmatrix} b & 0 \\ 0 & a \end{bmatrix}, \quad a = 0.8958, \quad b = 1.09659 \tag{3.1}$$

The stress-free strains are defined by $\boldsymbol{E}_1 = \dfrac{1}{2}\left(\boldsymbol{U}_1^2 - \boldsymbol{I}\right)$ and $\boldsymbol{E}_2 = \dfrac{1}{2}\left(\boldsymbol{U}_2^2 - \boldsymbol{I}\right)$. This twinning system admits stress-free compatible twinning interfaces with (referential) normal given by $\dfrac{1}{\sqrt{2}}\left(\boldsymbol{e}_1 \pm \boldsymbol{e}_2\right)$ where $\boldsymbol{e}_1, \boldsymbol{e}_2$ are the unit vectors in the Cartesian directions [4, 15, 19].

We assume that the elasticity tensor $\boldsymbol{C}$ is isotropic and identical in both phases, and set the extensional modulus to $206\mathrm{GPa}$ and the Poisson ratio to 0.3.

To set up the initial condition for dynamic calculations described later on, we obtain a stress-free compatible interfaces by setting $\phi = 1$ on the right of the domain and $\phi = 0$ on the left side, and then minimize the energy in (2.1). The resulting static twin interface is shown in Figure 1.

3.B. Nucleation Model

We first find the hyperplane in strain space that separates the twinning phases. Considering strains corresponding to the stretch tensors given in (3.1), the hyperplane that is the set of points that are of equal distance from $\boldsymbol{E}_1$ and $\boldsymbol{E}_2$ has the equation $|\boldsymbol{E}^* - \boldsymbol{E}_2| = |\boldsymbol{E}^* - \boldsymbol{E}_1|$. Solving for $\boldsymbol{E}^*$ gives $E^*_{11} = E^*_{22}$ as the equation of the hyperplane. On one side of the hyperplane, we are closer to $\boldsymbol{E}_1$ and ϕ should be less than 0.5; on the other side, we are closer to $\boldsymbol{E}_2$ and require that ϕ is greater than 0.5 (Fig. 2).

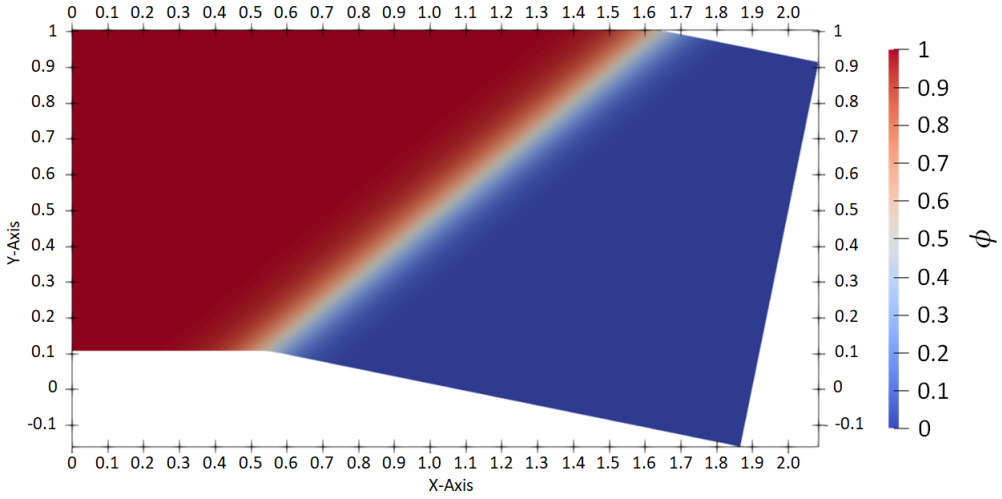

Figure 1. The deformed configuration of a rectangular block of size 2×1 with ϕ overlaid, after energy minimization with traction-free boundary conditions all around except for the horizontal displacement set to 0 on the left edge.

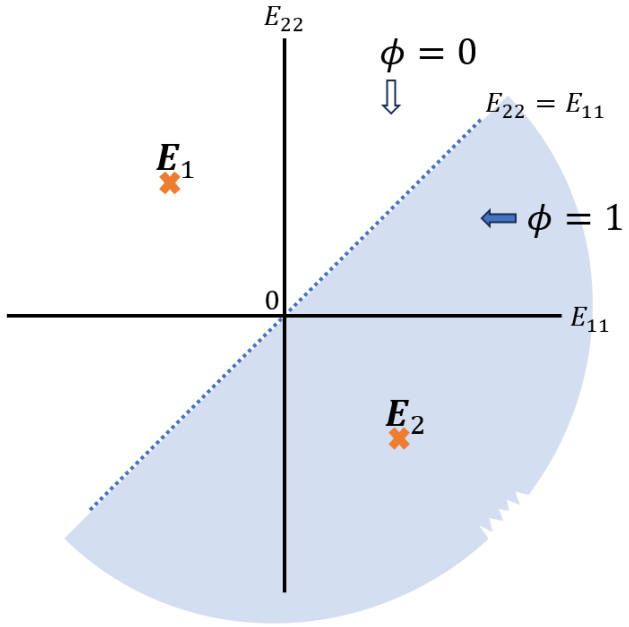

Figure 2. Schematic depiction of the correspondence between the strain $\boldsymbol{E}$ and the phase ϕ. We need $\phi < 0.5$ when $E_{22} > E_{11}$ and $\phi > 0.5$ when $E_{22} < E_{11}$.

We set up the nucleation criterion to enforce this correspondence, i.e., if we cross the hyperplane in strain space, we ensure that ϕ evolves appropriately. Specifically, the nucleation process must drive ϕ to below 0.5 when $E_{22} - E_{11} > 0$, and drive ϕ to above 0.5 when $E_{22} - E_{11} < 0$, which results in constructing a nucleation term of the form:

$$G(\boldsymbol{E}, \phi) = G_0\big(H_l\left(0.5 - \phi\right) H_l\left(E_{11} - E_{22}\right) - H_l\left(\phi - 0.5\right) H_l\left(E_{22} - E_{11}\right)\big) \tag{3.2}$$

Since the role of kinetics is not the central focus here, we use the simple linear form $\hat{v}\left(f\right) = \kappa f$. We use $\kappa = 1$ for the numerical calculations.

3.C. Results

We perform dynamic calculations using the boundary conditions shown in Figure 3. The boundary conditions are set up to minimally constrain the deformation of the body, and this allows a rigid vertical translation mode, but this mode does not interfere

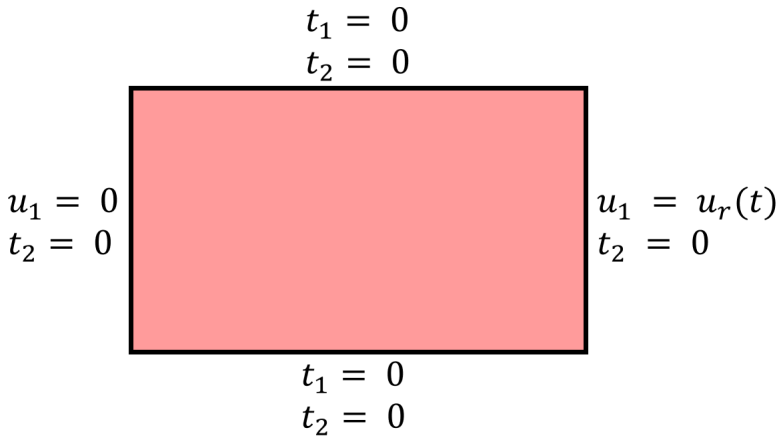

Figure 3. Boundary conditions, where t_1, t_2 refer to Cartesian components of traction, and u_1, u_2 refer to Cartesian components of the displacement. The prescribed time-dependent loading is $u_r(t)$.

with our observation of the twinning deformation. We use the static equilibrium interface as the initial conditions (Fig. 1).

Figure 4 provides a representative example that highlights the effect of the nucleation term. The highlight of the calculations shown in Figure 4 is that even at subsonic velocities, it is apparent that accounting for nucleation has a very significant effect and dominates over interface kinetics. Further, it shows that nonphysical regions in the energy landscape were accessed when nucleation is not accounted for.

We also note that the calculations in Figure 4 do not have viscosity, but the calculations with viscosity ($\eta = 1 \times 10^{-9}$s) are essentially identical. This overall conclusion holds for all the calculations described in this section.

For greater insight into the role of nucleation, Figure 5 plots the strain fields in a specimen where the nucleation term is inactive, i.e., the twinning transformation occurs exclusively due to interface motion and not nucleation. Looking at a time at which the calculation in Figure 4 that allows nucleation had nucleated several new domains, Figure 5 shows clearly that $E_{11} > E_{22}$ in the right part of the specimen. We would thus expect the $\phi = 1$ phase to nucleate in that region.

Figure 6 shows the driving force for nucleation G as a function of position, at a time when nucleation is active. We observe the value of G is very high in the lower right part of the specimen.

Comparing systems with and without nucleation, we observe in Figure 7 that the driving force for nucleation G drove the nucleation of the $\phi = 1$ phase in the right of the specimen, which corresponds to the position where the value of G was very high several timesteps ago. This suggests that the driving force for nucleation has driven the system to a physical region of the energy landscape.

A final point is that when we attempt to drive the interface to propagate faster (via higher loading rates), we encounter pinning — essentially, very slow evolution — of the interface where it meets the boundary of the specimen. As the twin phases are related by a shear, the driving force for the interface to propagate is related to the shear traction on the plane that is parallel to the interface. The boundaries are traction-free on the top and bottom of the domain, resulting in zero shear stress at the twin interface on the top and bottom boundary. This effectively pins the interface at the boundaries by causing it to evolve very slowly compared to the interior. This is further discussed in [5].

4. Anisotropic Kinetics Drives Needle Twin Growth

When twins initially nucleate, they grow in a characteristic needle-like geometry, e.g. the experimental observations in [10]. The growth of needle twins was studied using a sharp-interface model using theoretical approaches in several works by P. Rosakis [41, 46, 47]. A key finding in that body of work was that anisotropic kinetics is essential to capture needle-like twins. As discussed in [47], the incompatible direction should have more twinning dislocations then the compatible directions to accommodate the deformation, and hence the kinetics will be significantly different for twin motion along compatible and incompatible directions. This micromechanical effect gives rise to mesoscale anisotropy in the kinetics.

We aim to develop a phase-field description that can capture the phenomenon of needle twin growth. A key challenge for standard phase-field models is the inability to incorporate anisotropic kinetics. We develop a phase-field model here that has anisotropic kinetics and show that it is able to capture needle-like twin growth, but also show that incorporating nucleation is essential to prevent nonphysical broadening. Following [27], we work in the antiplane elastic setting for simplicity.

4.A. Model Formulation

We work in the 2-d anti-plane setting. The independent space variable is denoted $\boldsymbol{x} = (x_1, x_2)$ in Cartesian coordinates; and the displacement has a single non-zero component in the out-of-plane 3-direction, denoted $u(\boldsymbol{x}, t)$ where t is the time. The strain is

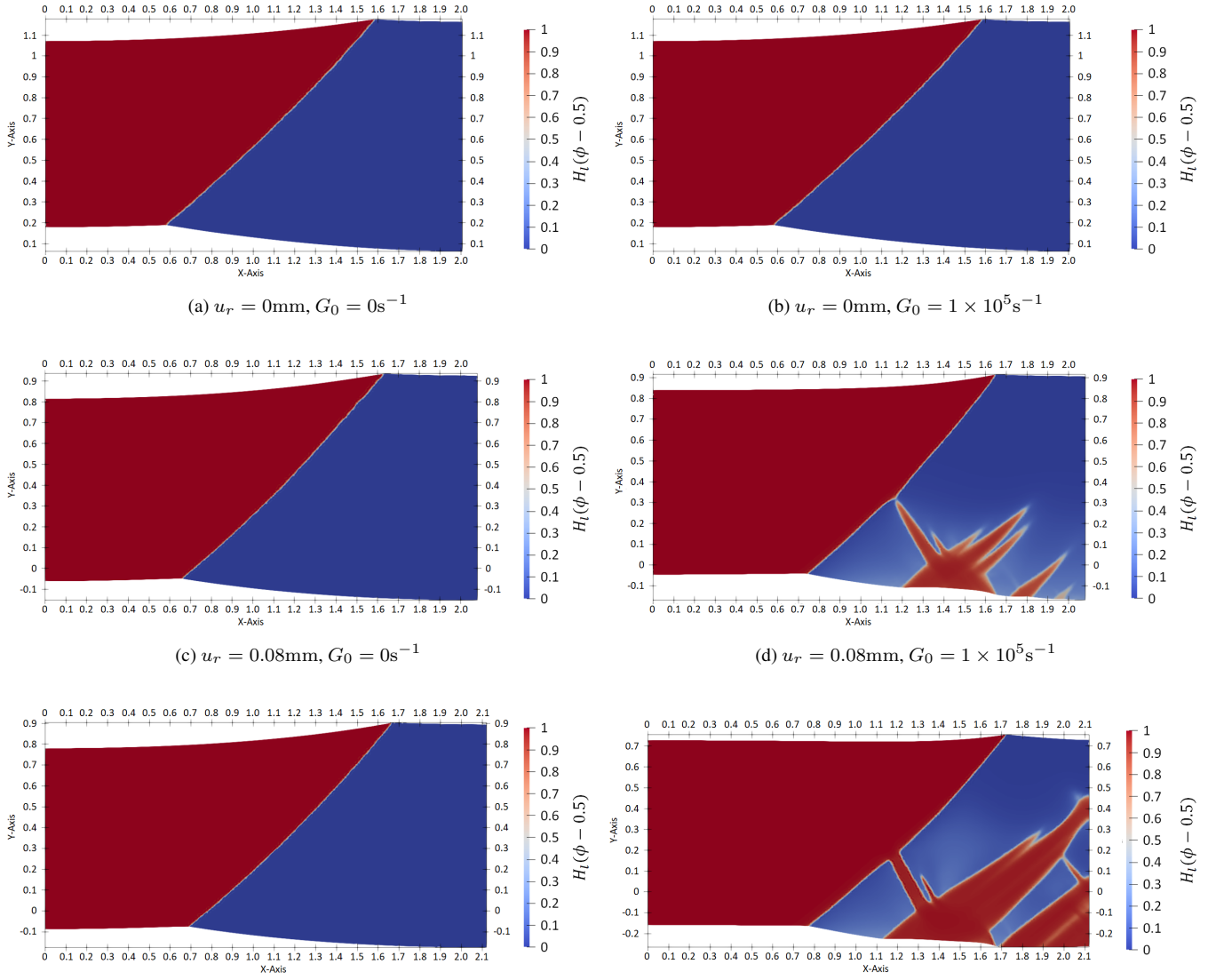

(a) $u_r = 0\text{mm}$, $G_0 = 0\text{s}^{-1}$

(b) $u_r = 0\text{mm}$, $G_0 = 1 \times 10^5\text{s}^{-1}$

(c) $u_r = 0.08\text{mm}$, $G_0 = 0\text{s}^{-1}$

(d) $u_r = 0.08\text{mm}$, $G_0 = 1 \times 10^5\text{s}^{-1}$

(e) $u_r = 0.12\text{mm}$, $G_0 = 0\text{s}^{-1}$

(f) $u_r = 0.12\text{mm}$, $G_0 = 1 \times 10^5\text{s}^{-1}$

Figure 4. Plots of the deformed configuration overlaid with the phase evolution given by $H_l(\phi - 0.5)$. The left column is without nucleation and the right column considers nucleation. The first row depicts the initial condition, and the second and third rows depict the evolution in time. The imposed loading corresponds to $u_r(t) = \left(1 \times 10^3 \text{mm}\,\text{s}^{-1}\right) t$. We see that accounting for nucleation has a very significant impact on twinning transformation, with large regions well ahead of the moving interface transforming due to nucleation. That is, nucleation significantly dominates kinetics.

denoted $\boldsymbol{\varepsilon}$, and has only two non-zero components: $\varepsilon_1 = \frac{1}{2}\partial_{x_1} u$ and $\varepsilon_2 = \frac{1}{2}\partial_{x_2} u$.

We use displacement boundary conditions all around and use this to simulate dynamic loading. We start with a single phase and have a small nucleus (of size 0.05) of the second phase near one of the vertical edges to drive the growth of a single needle twin in a convenient location.

4.A.1. Elasticity

We set each phase to have the quadratic form:

$$W_i(\boldsymbol{\varepsilon}) = \tfrac{1}{2}\mu|\boldsymbol{\varepsilon} - \boldsymbol{\varepsilon}_{0i}|^2 \tag{4.1}$$

The material is isotropic in the antiplane setting; see [46] for discussion on the anisotropic case. We use $\mu = 1$.

The stress-free strains are $\boldsymbol{\varepsilon}_{01} = \mathbf{0}$ and $\boldsymbol{\varepsilon}_{02} = \{0.0, 1.0\}$. Consequently, the compatible direction is $\boldsymbol{n} = \boldsymbol{e}_2 = \{0, 1\}$.

For viscous dissipation, we use $\eta\dot{\boldsymbol{\varepsilon}}$ with $\eta = 0.005$.

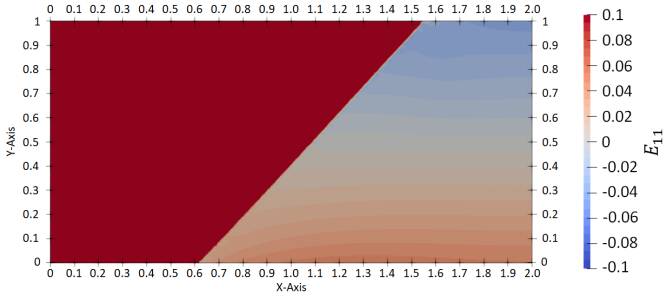

(a) E_{11}

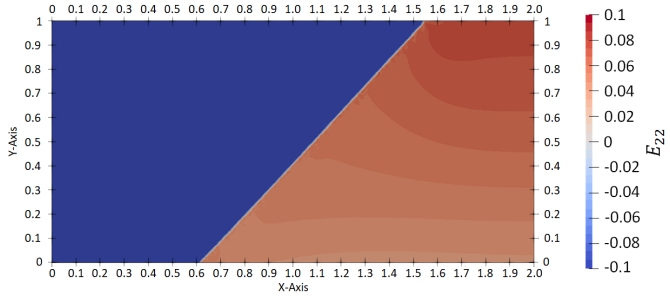

(b) E_{22}

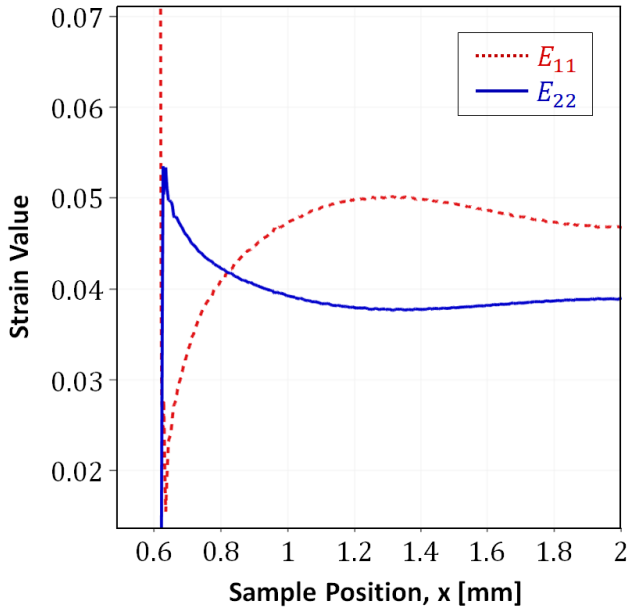

(c) Line plot of E_{11} and E_{22} along the horizontal centerline.

Figure 5. Plots of E_{11} and E_{22} at $u_r = 0.18\text{mm}$ with a loading rate $u_r(t) = \left(1 \times 10^3 \text{mm}\,\text{s}^{-1}\right) t$, with nucleation suppressed. The system reaches nonphysical regimes in the energy landscape, i.e., the strain and ϕ are not consistent with Figure 2, and this would drive nucleation.

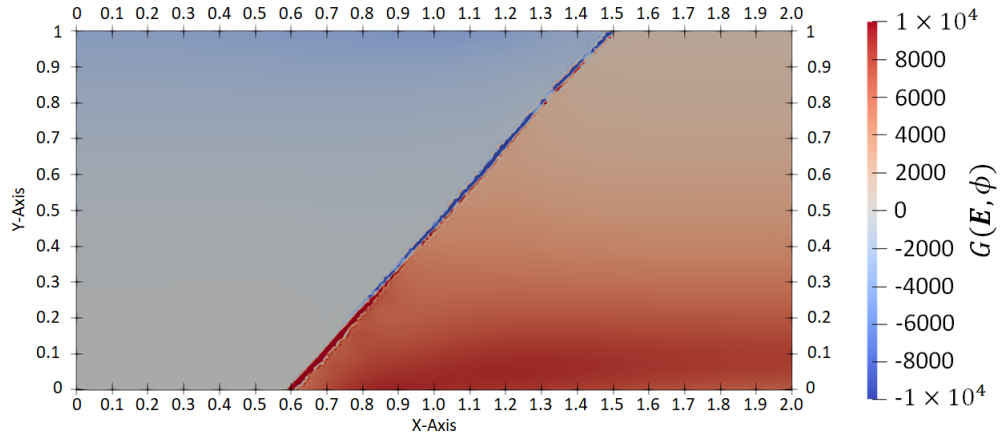

Figure 6. The driving force for nucleation over the specimen, with $u_r = 0.04\text{mm}$ with $G_0 = 1 \times 10^5 \text{s}^{-1}$.

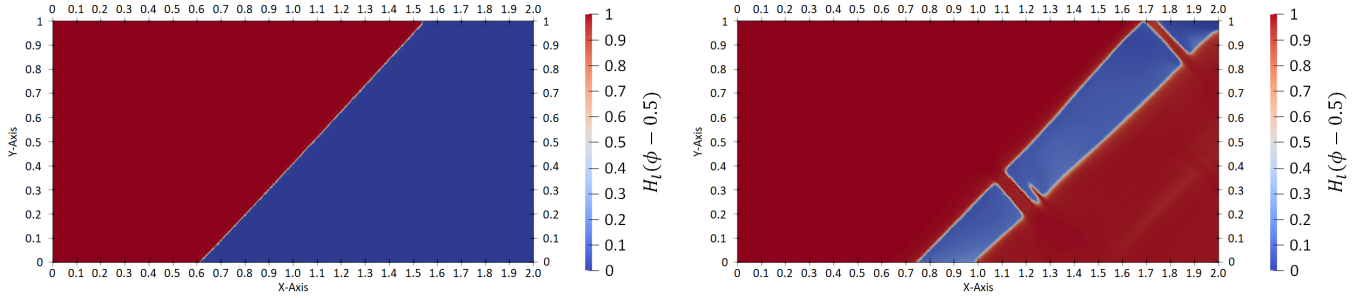

(a) $u_r = 0.18\text{mm}$, $G_0 = 0\text{s}^{-1}$ (b) $u_r = 0.18\text{mm}$, $G_0 = 1 \times 10^5\text{s}^{-1}$

Figure 7. Plots of $H_l(\phi - 0.5)$ for a system (a) without nucleation and (b) with nucleation, with a loading rate $u_r(t) = \left(1 \times 10^3 \text{mm}\,\text{s}^{-1}\right) t$. Comparing against the line plot in Figure 5(c), we see that nucleation has driven twinning through much of the right side of the specimen.

4.A.2. Anisotropic kinetics

We use isotropic kinetics and anisotropic kinetics with the respective forms below:

$$\hat{v} = \kappa f \tag{4.2}$$

$$\hat{v} = \kappa f \left(0.1 + \frac{|\nabla\phi \cdot \boldsymbol{a}|}{|\nabla\phi|}\right) \tag{4.3}$$

In the anisotropic form, there are two terms in the parentheses: the first is isotropic, and the second introduces anisotropy by its dependence on the interface normal $\nabla\phi$. It models faster kinetics for portions of the interface that have normal closer to the $\boldsymbol{a}$ direction; we set $\boldsymbol{a} = \boldsymbol{e}_1$ for the numerical calculations. Further, we use $\kappa = 5.0$.

4.A.3. Nucleation

The nucleation term has the following form:

$$G(\boldsymbol{\varepsilon}, \phi) = G_0 \left(H_l\left(\phi - 0.5\right)\left(H_l\left(\varepsilon_2 - \bar{\varepsilon}\right) - 1\right) + \left(1 - H_l\left(\phi - 0.5\right)\right) H_l\left(\varepsilon_2 - \bar{\varepsilon}\right)\right) \tag{4.4}$$

where $\bar{\varepsilon} = 0.5$.

4.B. Comparing Isotropic and Anisotropic Kinetics

We begin by examining effect of anisotropic kinetics, but do not account for nucleation to enable us to precisely understand their separate roles.

Figure 8 shows the evolution of the twin needle in time, comparing isotropic kinetics to anisotropic kinetics. We see that anisotropy is essential to obtain needle-like twin growth, consistent with the work of [47]. However, we also notice that the twin slowly gets wider in the thin direction beginning at the base.

4.C. Effect of Nucleation and Viscous Stress

Building on the observation that anisotropic kinetics appears essential to predict realistic needle twins, we next consider the effect of further accounting for viscous stress and nucleation. Figure 9 compares the effect of accounting for nucleation and viscous stresses in addition to anisotropic kinetics. We see that viscous stresses attenuate the leading elastic waves but do not significantly affect the needle twin microstructure. In contrast, the nucleation term serves the important purpose of suppressing the nonphysical broadening of the twin.

We further plot the driving forces for kinetics and nucleation in Figure 10. First, we notice that both driving forces are of comparable magnitude. Second, we highlight that the nucleation term is active at the growing tip as expected, but also at the base of the needle twin where it acts to prevent nonphysical twin broadening.

4.D. Supersonic Twin Growth

We next look at the role of nucleation and viscous stress in supersonic twinning. To prevent the use of overly large stresses, we achieve supersonic twinning by increasing the kinetic coefficient κ by a factor of 10. Figure 11 compares the twin microstructure in a model with only anisotropic kinetics to a model that also accounts for nucleation and viscous stress. As can be inferred from the Mach cone structure, both twins grow supersonically, with the model with viscous damping showing faster twin growth.

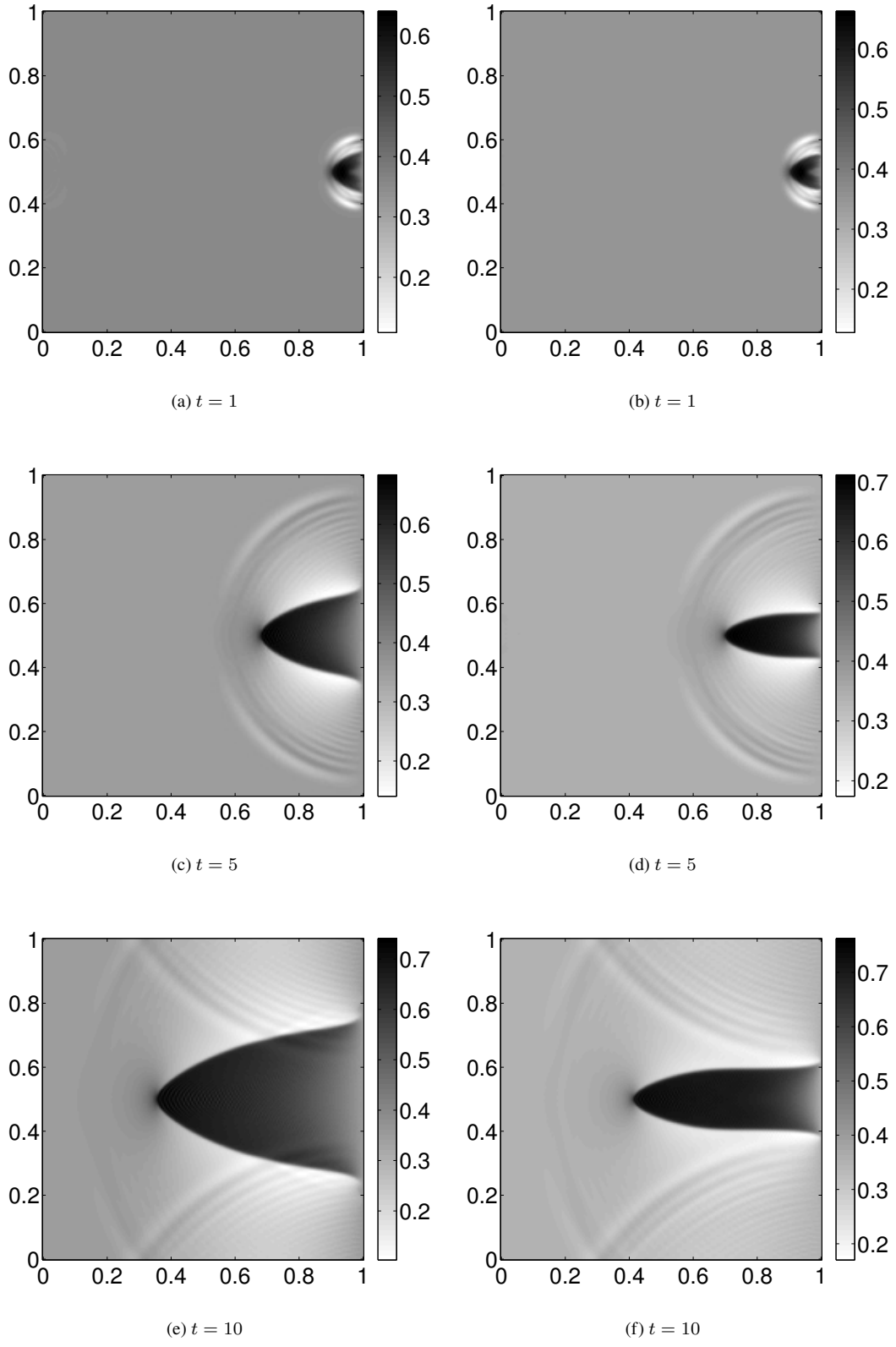

(a) $t = 1$ (b) $t = 1$

(c) $t = 5$ (d) $t = 5$

(e) $t = 10$ (f) $t = 10$

Figure 8. Time evolution of ε_2 ($t = 1, 5, 10$). The left and right columns are respectively isotropic and anisotropic kinetics, with faster propagation when the local interface normal is closer to being aligned with $\boldsymbol{e}_1$.

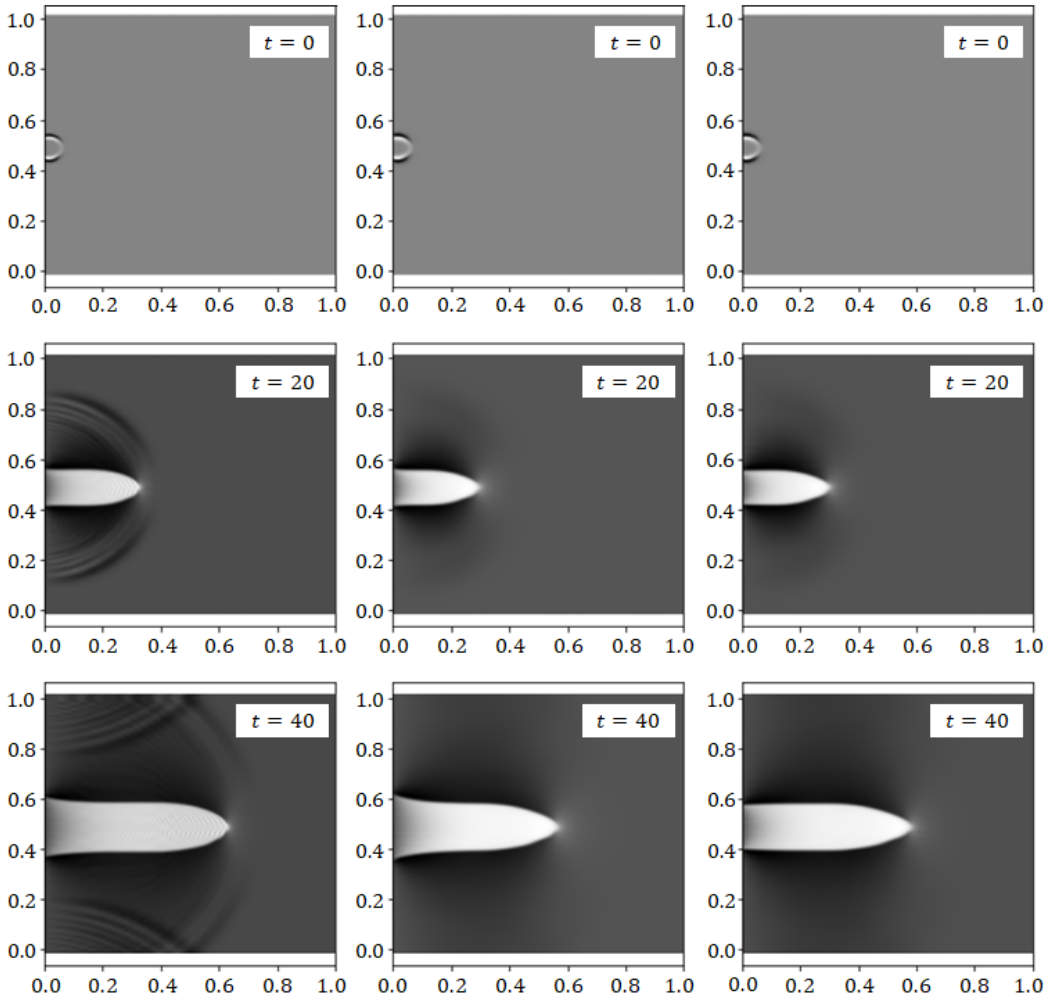

Figure 9. Time evolution of ε_2 ($t = 0, 20, 40$). The left column accounts only for anisotropic kinetics; the middle column includes also viscous stress; and the right column with anisotropic kinetics, viscous stress, and nucleation. We highlight that including viscous stress and nucleation appears to suppress the nonphysical broadening of the twin as it grows.

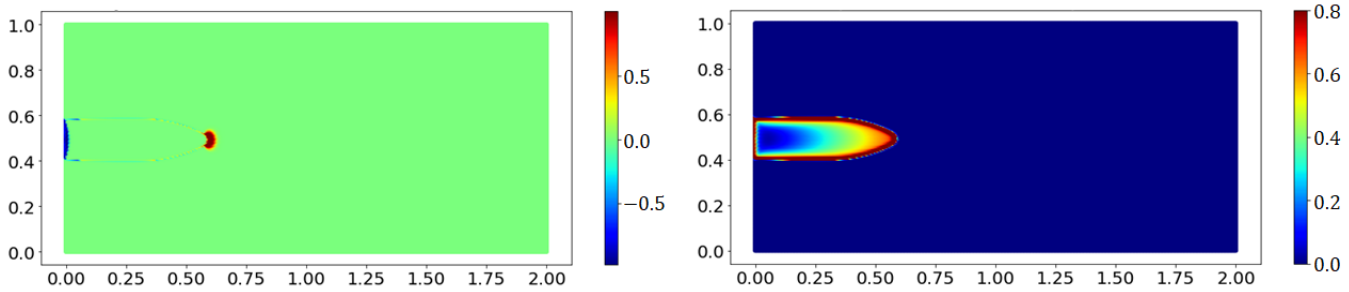

Figure 10. The driving force for nucleation (left) and kinetics (right) at $t = 40$. Both driving forces have comparable magnitudes, and the nucleation driving force acts at the base of the needle twin to prevent nonphysical broadening.

We next plot the kinetic driving force for both models in Figure 12, and notice that there are no significant differences. As expected in our class of models, the driving force is localized around the moving interface [5, 11].

Figure 13 shows the nucleation driving force and the viscous stress. We notice that both are highly localized at the tip of the growing twin, and that the largest value of the nucleation driving force is comparable to the kinetic driving force.

Remark 4.1 (Supersonic Twinning with Unequal Moduli)**.** We have performed similar supersonic twinning calculations for the

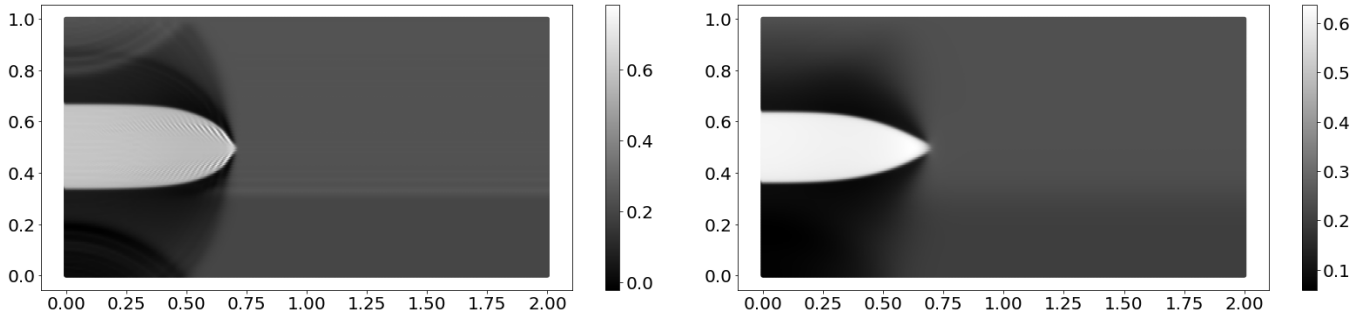

Figure 11. Supersonic twin growth needles visualized through plotting ε_2 ($t = 40$). The left figure accounts only for anisotropic kinetics and predicts a somewhat-rounded twin growing at Mach 1.06. The right figure accounts further for nucleation and viscous stress, and predicts a more needle-like twin that grows slightly faster at Mach 1.13.

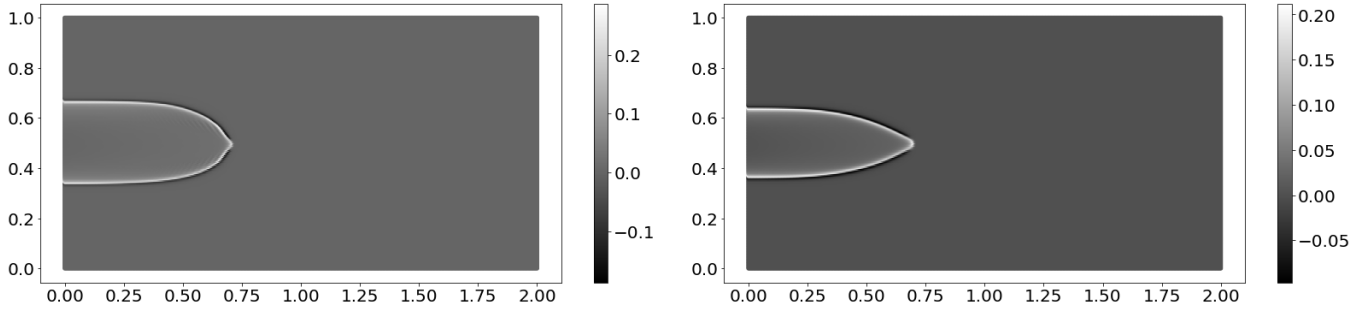

Figure 12. The kinetic driving force in the model without (left) and with (right) nucleation and viscous stress.

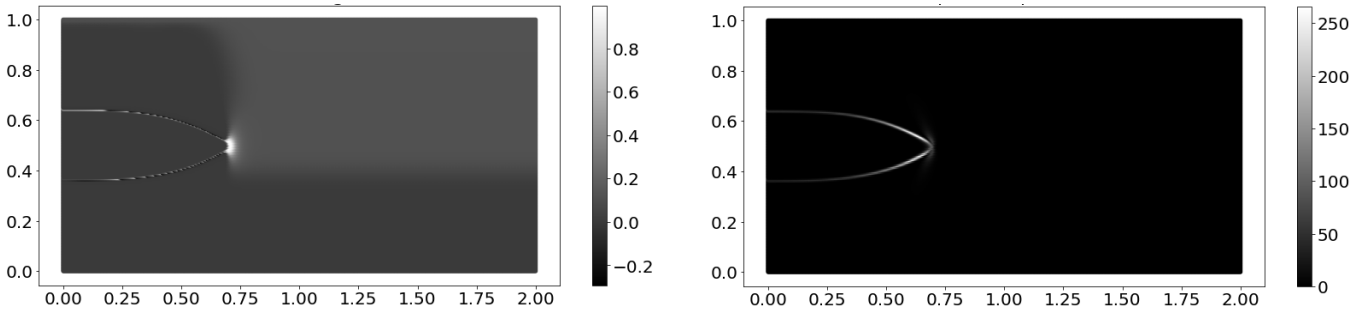

Figure 13. Left: the driving force for nucleation, which has magnitude comparable to the kinetic driving force (Fig. 12). Right: the viscous stress. Both are highly localized at the growing tip of the needle twin.

case where the moduli are unequal with the ratio $1 : 4$. When the twin propagates into the soft phase, the results are qualitatively similar to the discussion above. When the twin propagates into the stiff phase, the needle twin appears unstable and splits up into a more complex microstructure. □

5. Discussion

We have used a recent phase-field modeling framework proposed in [5, 6, 11] to study the interplay between kinetics and nucleation in the dynamic evolution of twins. The ability of this framework to explicitly and transparently specify nucleation and kinetic behavior is essential to model phenomena such as needle twin growth. For instance, anisotropic interface kinetics is essential to model needle twin growth, but it is unclear how — or if it is even possible — to specify anisotropic kinetics in standard phase-field approaches or alternatives such as peridynamics.

For the problems studied in this paper, we find that viscous stresses do not play an important role. This is a significant difference compared to studies in other settings, e.g., [11, 22]. In contrast to those works, the process of twinning in higher dimensions is

dominated by geometric compatibility, which leads to this significant difference.

Software and Data Availability. The code developed for this work and the associated data are available at `https://github.com/janelchua/Phase-field_Twin-interface`

Acknowledgments. We thank NSF (2108784, 2012259) and ARO (MURI W911NF-19-1-0245) for support; NSF for XSEDE computing resources provided by Pittsburgh Supercomputing Center; Maryam Khodadad for reviewing the code; and Tony Rollett and Phoebus Rosakis for useful discussions.

[1] Rohan Abeyaratne and James K Knowles. On the driving traction acting on a surface of strain discontinuity in a continuum. *Journal of the Mechanics and Physics of Solids*, 38(3):345–360, 1990.

[2] Rohan Abeyaratne and James K Knowles. Implications of viscosity and strain-gradient effects for the kinetics of propagating phase boundaries in solids. *SIAM Journal on Applied Mathematics*, 51(5):1205–1221, 1991.

[3] Rohan Abeyaratne and James K Knowles. Kinetic relations and the propagation of phase boundaries in solids. *Archive for rational mechanics and analysis*, 114(2):119–154, 1991.

[4] Rohan Abeyaratne and James K Knowles. *Evolution of phase transitions: a continuum theory*. Cambridge University Press, 2006.

[5] Vaibhav Agrawal and Kaushik Dayal. A dynamic phase-field model for structural transformations and twinning: Regularized interfaces with transparent prescription of complex kinetics and nucleation. part i: Formulation and one-dimensional characterization. *Journal of the Mechanics and Physics of Solids*, 85:270–290, 2015.

[6] Vaibhav Agrawal and Kaushik Dayal. A dynamic phase-field model for structural transformations and twinning: Regularized interfaces with transparent prescription of complex kinetics and nucleation. part ii: Two-dimensional characterization and boundary kinetics. *Journal of the Mechanics and Physics of Solids*, 85:291–307, 2015.

[7] Vaibhav Agrawal and Kaushik Dayal. Dependence of equilibrium griffith surface energy on crack speed in phase-field models for fracture coupled to elastodynamics. *International Journal of Fracture*, 207:243–249, 2017.

[8] Hans-Dieter Alber and Peicheng Zhu. Solutions to a model with nonuniformly parabolic terms for phase evolution driven by configurational forces. *SIAM Journal on Applied Mathematics*, 66(2):680–699, 2005.

[9] Martin Alnaes, Jan Blechta, Johan Hake, August Johansson, Benjamin Kehlet, Anders Logg, Chris Richardson, Johannes Ring, Marie. E Rognes, and Garth N Wells. The fenics project version 1.5. *Archive of Numerical Software*, 3(100):9–23, 2015.

[10] W Cai, XL Meng, YF Zheng, JX Zhang, and LC Zhao. Interface structure and mobility in martensitic shape memory alloys. *Materials Science and Engineering: A*, 438:900–904, 2006.

[11] Janel Chua, Vaibhav Agrawal, Timothy Breitzman, George Gazonas, and Kaushik Dayal. Phase-field modeling and peridynamics for defect dynamics, and an augmented phase-field model with viscous stresses. *Journal of the Mechanics and Physics of Solids*, 159:104716, 2022.

[12] Janel Chua, Mina Karimi, Patrick Kozlowski, Mehrdad Massoudi, Santosh Narasimhachary, Kai Kadau, George Gazonas, and Kaushik Dayal. Deformation decomposition versus energy decomposition for chemo-and poro-mechanics. *Journal of Applied Mechanics*, 91(1): 014501, 2024.

[13] J.D. Clayton. Nonlinear eulerian thermoelasticity for anisotropic crystals. *Journal of the Mechanics and Physics of Solids*, 61(10):1983–2014, October 2013. ISSN 0022-5096. doi:10.1016/j.jmps.2013.05.009. URL `http://dx.doi.org/10.1016/j.jmps.2013.05.009`.

[14] J.D. Clayton, R.B. Leavy, and J. Knap. Phase field theory for pressure-dependent strength in brittle solids with dissipative kinetics. *Mechanics Research Communications*, 129:104097, May 2023. ISSN 0093-6413. doi:10.1016/j.mechrescom.2023.104097. URL `http://dx.doi.org/10.1016/j.mechrescom.2023.104097`.

[15] John D Clayton. *Nonlinear mechanics of crystals*, volume 177. Springer Science & Business Media, 2010.

[16] John D. Clayton. A universal phase-field mixture representation of thermodynamics and shock wave mechanics in porous soft biologic continua, 2024. URL `https://arxiv.org/abs/2403.04995`.

[17] John D Clayton and Jarek Knap. A phase field model of deformation twinning: nonlinear theory and numerical simulations. *Physica D: Nonlinear Phenomena*, 240(9):841–858, 2011.

[18] John D Clayton and Jarek Knap. A geometrically nonlinear phase field theory of brittle fracture. *International Journal of Fracture*, 189(2): 139–148, 2014.

[19] Kaushik Dayal and Kaushik Bhattacharya. Kinetics of phase transformations in the peridynamic formulation of continuum mechanics. *Journal of the Mechanics and Physics of Solids*, 54(9):1811–1842, September 2006. doi:10.1016/j.jmps.2006.04.001. URL `https://doi.org/10.1016/j.jmps.2006.04.001`.

[20] Kaushik Dayal and Kaushik Bhattacharya. A real-space non-local phase-field model of ferroelectric domain patterns in complex geometries. *Acta materialia*, 55(6):1907–1917, 2007.

[21] Eilon Faran and Doron Shilo. The kinetic relation for twin wall motion in nimnga. *Journal of the Mechanics and Physics of Solids*, 59(5): 975–987, 2011.

[22] Anshul Faye, José A Rodríguez-Martínez, and KY Volokh. Spherical void expansion in rubber-like materials: The stabilizing effects of viscosity and inertia. *International Journal of Non-Linear Mechanics*, 92:118–126, 2017.

[23] Alan D. Freed, Shahla Zamani, László Szabó, and John D. Clayton. Laplace stretch: Eulerian and lagrangian formulations. *Zeitschrift für angewandte Mathematik und Physik*, 71(5), August 2020. ISSN 1420-9039. doi:10.1007/s00033-020-01388-4. URL `http://dx.doi.org/10.1007/s00033-020-01388-4`.

[24] Eliot Fried and Morton E Gurtin. Dynamic solid-solid transitions with phase characterized by an order parameter. *Physica D: Nonlinear Phenomena*, 72(4):287–308, 1994.

[25] Laurent Guin and Dennis M Kochmann. A phase-field model for ferroelectrics with general kinetics, part i: Model formulation. *Journal of the Mechanics and Physics of Solids*, 176:105301, 2023.

[26] Maryam Hakimzadeh, Vaibhav Agrawal, Kaushik Dayal, and Carlos Mora-Corral. Phase-field finite deformation fracture with an effective energy for regularized crack face contact. *Journal of the Mechanics and Physics of Solids*, 167:104994, 2022.

[27] Thomas Y Hou, Phoebus Rosakis, and Philippe LeFloch. A level-set approach to the computation of twinning and phase-transition dynamics. *Journal of Computational Physics*, 150(2):302 – 331, 1999. ISSN 0021-9991. doi:http://dx.doi.org/10.1006/jcph.1998.6179. URL `http://www.sciencedirect.com/science/article/pii/S0021999198961794`.

[28] Shuyin Jiao and Yashashree Kulkarni. Molecular dynamics study of creep mechanisms in nanotwinned metals. *Computational Materials Science*, 110:254–260, 2015.

[29] Shuyin Jiao and Yashashree Kulkarni. Radiation tolerance of nanotwinned metals–an atomistic perspective. *Computational Materials Science*, 142:290–296, 2018.

[30] Mina Karimi, Mehrdad Massoudi, Noel Walkington, Matteo Pozzi, and Kaushik Dayal. Energetic formulation of large-deformation poroelasticity. *International Journal for Numerical and Analytical Methods in Geomechanics*, 46(5):910–932, 2022.

[31] Mina Karimi, Mehrdad Massoudi, Kaushik Dayal, and Matteo Pozzi. High-dimensional nonlinear bayesian inference of poroelastic fields from pressure data. *Mathematics and Mechanics of Solids*, 28(9):2108–2131, 2023.

[32] Alain Karma, David A Kessler, and Herbert Levine. Phase-field model of mode iii dynamic fracture. *Physical Review Letters*, 87(4): 045501, 2001.

[33] Yashashree Kulkarni and Robert J Asaro. Are some nanotwinned fcc metals optimal for strength, ductility and grain stability? *Acta Materialia*, 57(16):4835–4844, 2009.

[34] Anders Logg, Kent-Andre Mardal, and Garth Wells. *Automated Solution of Differential Equations by the Finite Element Method*. Springer, 2012.

[35] S Kiana Naghibzadeh, Noel Walkington, and Kaushik Dayal. Surface growth in deformable solids using an eulerian formulation. *Journal of the Mechanics and Physics of Solids*, 154:104499, 2021.

[36] S Kiana Naghibzadeh, Noel Walkington, and Kaushik Dayal. Accretion and ablation in deformable solids with an eulerian description: examples using the method of characteristics. *Mathematics and Mechanics of Solids*, 27(6):989–1010, 2022.

[37] Oliver Penrose and Paul C Fife. Thermodynamically consistent models of phase-field type for the kinetic of phase transitions. *Physica D: Nonlinear Phenomena*, 43(1):44–62, 1990.

[38] David A Porter and Kenneth E Easterling. *Phase transformations in metals and alloys (revised reprint)*. CRC press, 2009.

[39] Phoebus Rosakis. An equal area rule for dissipative kinetics of propagating strain discontinuities. *SIAM Journal on Applied Mathematics*, 55(1):100–123, 1995.

[40] Phoebus Rosakis and James K Knowles. Unstable kinetic relations and the dynamics of solid-solid phase transitions. *Journal of the Mechanics and Physics of Solids*, 45(11):2055–2081, 1997.

[41] Phoebus Rosakis and Hungyu Tsai. Dynamic twinning processes in crystals. *International journal of solids and structures*, 32(17-18): 2711–2723, 1995.

[42] Yasemin Şengül. Nonlinear viscoelasticity of strain rate type: an overview. *Proceedings of the Royal Society A*, 477(2245):20200715, 2021.

[43] Tanushree Sinha and Yashashree Kulkarni. Alternating brittle and ductile response of coherent twin boundaries in nanotwinned metals. *Journal of Applied Physics*, 116(18), 2014.

[44] LM Truskinovskii. Equilibrium phase interfaces. In *Sov. Phys. Dokl*, volume 27, pages 551–552, 1982.

[45] Lev Truskinovsky. Kinks versus shocks. In *Shock induced transitions and phase structures in general media*, pages 185–229. Springer, 1993.

[46] Hungyu Tsai and Phoebus Rosakis. On anisotropic compressible materials that can sustain elastodynamic anti-plane shear. *Journal of Elasticity*, 35(1):213–222, 1994.

[47] Hungyu Tsai and Phoebus Rosakis. Quasi-steady growth of twins under stress. *Journal of the Mechanics and Physics of Solids*, 49(2):289 – 312, 2001. ISSN 0022-5096. doi:http://dx.doi.org/10.1016/S0022-5096(00)00035-1.

[48] Sergio Turteltaub. Viscosity of strain gradient effects on the kinetics of propagating phase boundaries in solids. *Journal of elasticity*, 46(1): 53–90, 1997.

[49] Lun Yang and Kaushik Dayal. Formulation of phase-field energies for microstructure in complex crystal structures. *Applied Physics Letters*, 96(8), 2010.